ELSEVIER

Journal of Nuclear Materials 307–311 (2002) 144–148

journal of nuclear materials

www.elsevier.com/locate/jnucmat

Non-destructive testing of CFC monoblock divertor mock-ups

K. Ezato *, M. Dairaku, M. Taniguchi, K. Sato, M. Akiba

Japan Atomic Energy Research Institute, Naka Fusion Research Establishment, 801-1, Mukoyama, Naka-machi, Naka-gun, Ibaraki 311-0193, Japan

Abstract

Non-destructive examination (NDE) methods for joint interfaces between different materials in high heat flux (HHF) components of divertor should be urgently developed to assure quality and reliability of joining techniques. The purpose of this work is to demonstrate the ability of using ultrasonic wave and thermography NDE techniques to detect the defect in the joining interface (joint defect) of divertor mock-ups with carbon-fiber reinforced carbon monoblock armor tiles brazed on a copper cooling tube. The results of both NDEs are benchmarked with HHF tests and cross-sectional observation of the mock-up to correlate the joint defect size detected with NDEs to the thermal response of the mock-up with initial joint defects. From the results of the HHF tests and the cross-sectional observations, it can be concluded that both NDE techniques have sufficient accuracy to predict the surface temperature of the HHF components.

1. Introduction

The non-destructive examination (NDE) method is one of the key issues in developing plasma-facing components (PFCs) for a next generation fusion devices such as ITER. In PFCs for ITER, armor tiles made of refractory materials are metallurgically bonded to the cooling structure to avoid the heat resistance between them. In particular, NDE methods for the bonding interfaces of the divertor, where carbon-fiber reinforced carbon (CFC) monoblock armor tiles are brazed on the cooling tube made of Cu-alloys [1], should be urgently developed to assure quality and reliability of the bonding techniques. From the viewpoint of the inspection cost, two NDE methods are considered as promising NDE methods for PFCs; one is ultrasonic testing [2,3] and the other is thermography [4,5]. In the former method, an ultrasonic wave is drastically damped in CFC armor because of its high porosity. For this reason, the ultrasonic testing from the cooling side tube has been intensively developed and the feasibility of this method has been demonstrated. The latter method is based on infrared (IR) measurements of surface temperatures of armor tiles during thermal transient produced by cold water flowing to the test element warmed-up by hot water.

At the present stage, however, only a few NDE data related to PFCs with a CFC monoblock concept exist to the authors' knowledge [2,6,7]. The goal of this study is to establish criteria of NDEs for CFC monoblocks brazed on copper cooling tubes. For this purpose, we investigated both NDE methods to check their detection ability of the initial defect in the joint interface (joint defect) on identical divertor mock-ups with CFC. The results were benchmarked against the high heat flux (HHF) tests and cross-sectional observations carried out using these divertor mock-ups.

2. Test procedures and results of NDEs

2.1. Test mock-up with CFC monoblocks

Two divertor mock-ups, TP-1 and TP-2, with CFC monoblocks for NDEs and HHF tests were fabricated as shown in Fig. 1. The mock-ups had five 2-D CFC

* Corresponding author. Tel.: +81-29 270 7552; fax: +81-29 270 7559.

E-mail address: ezatok@fusion.naka.jaeri.go.jp (K. Ezato).

0022-3115/02/$ - see front matter
PII: S0022-3115(02)01033-4

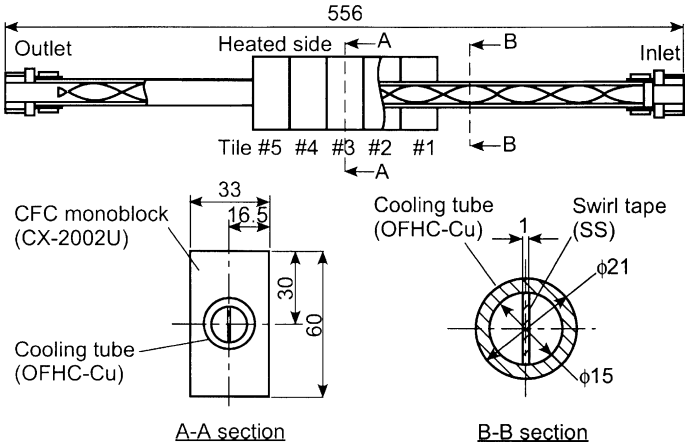

Fig. 1. Details of CFC monoblock diverter mock-up.

(CX-2002U, Toyo-Tanso Ltd.) armor files which were brazed on the cooling tube made of oxygen-free high-conductivity Cu with an inner diameter of 15 mm and an outer diameter of 21 mm. The brazing filler was as Ag–Cu–Ti alloy and the brazing temperature was 980 °C. A removable twisted tape made of stainless steel with a twisted ratio of three was inserted and fixed by a sleeve at the entrance of the cooling tube.

2.2. Test procedures for NDE with thermography

A systematic verification of the thermal continuity of the joint interface of the mock-ups was performed using transient thermographic measurements. Details of the set-up and procedures for these measurements are reported elsewhere [8]. The mock-up was warmed up to 90 °C before flowing the cold water with an axial velocity of 2.8 m/s and an inlet temperature of 30 °C. The surface temperatures of the mock-ups were measured with an IR camera. IR images were stored with a frame rate of 30 frames/s. Fig. 2 shows the IR images of TP-1 at 4 s after the start of cooling. The tiles could be identified in the number order (1–5) from the upstream of the cooling water.

To estimate the size of the joint defect in the present study, the thermal time constant of the armor tiles during the cooling phase were compared with results of numerical analyses. To evaluate the thermal time constant, a normalized temperature T^* was derived from the measured temperatures with the equation $T^* = (T - T_{\min})/(T_{\max} - T_{\min})$, where T is the measured surface temperature, $T_{\min}$ and $T_{\max}$ are the minimum and maximum temperatures during the cooling phase. Because of the high thermal conductivity of CFC, differences of T^* between the center point and the edge of the tiles were not significant during the cooling phase. Therefore, the thermal time constant was evaluated at the center point of each tile. Typical T^* response during the cooling phase is compared with the results of two-dimensional finite element (FE) calculations [8] using the ABAQUS code [10] as shown in Fig. 3. The thermal time constant of the armor tile, $\Delta\tau$, is defined with the equation, $\Delta\tau = \tau(T^* = 0.95) - \tau(T^* = 0.5)$, where $\tau(T^*)$ is the elapsed time at which T^* becomes 0.95 or 0.5 as shown in Fig. 3. Using this $\Delta\tau$, we could compare numerically the thermal response of each tile with the FE analyses. In these analyses, the joint defect was assumed to be symmetric and longitudinal at the upper heated side of the joint interface.

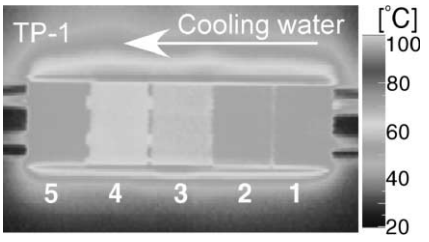

Fig. 2. IR images of TP-1 at 4 s after start of cooling.

2.3. Results of NDE with thermography

Table 1 shows the joint defect sizes of the tiles of the mock-ups based on the results of the NDE with thermography. In the present study, the joint defect size is defined as the ratio of the joint defect length to the circumference of the joint interface. Then, the joint defect size was determined by correlating $\Delta\tau$ to an interpolation of the FE calculations as shown in Fig. 4 with dotted lines. For instance, tiles #1 and #5 of TP-1 had almost the same $\Delta\tau$ as those of the FE calculation without any joint defect. On the contrary, tiles #3 and #4 had worse thermal time constants, 3.1 and 3.3 s, respectively, which corresponded to calculated joint defects of 26.4% and 29.2%.

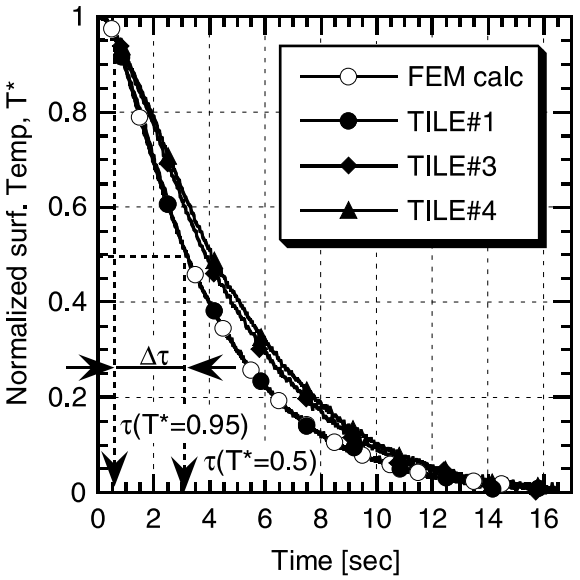

Fig. 3. Normalized surface temperatures of tiles #1, #3 and #4 of TP-1 compared with FE analyses and definition of thermal time constant, $\Delta\tau$.

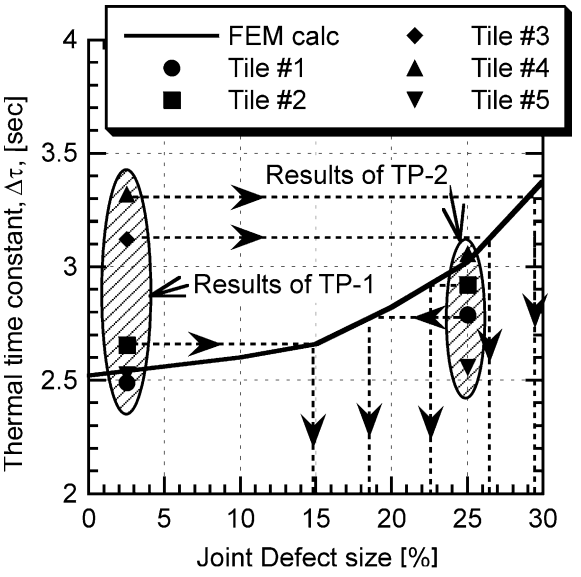

Fig. 4. Estimation of joint defect size for the CFC monoblock armor tiles of TP-1 and TP-2. Dotted lines in this figure are examples of estimation of joint defect size in each tile of TP-1 and TP-2 with interpolation of FE calculations.

Table 1
Joint defect size (%) estimated with thermographic NDE

Mock-up	Tile #1	Tile #2	Tile #3	Tile #4	Tile #5
TP1	0.0	14.7	26.4	29.2	0.4
TP2	19.0	22.5	22.5	25.5	4.6

2.4. Test procedures for NDE with ultrasonic wave

A test stand to conduct the ultrasonic testing was set-up in JAERI to characterize the joint interfaces of the CFC monoblocks and the cooling tube of the mock-ups. Details of this test stand and procedures of the present ultrasonic testing are reported elsewhere [8]. The transducer used in the present study was designed to locate the focus point of the ultrasonic pulse at the joint interface of the mock-up [9]. The resonance frequency of the transducer was designed to be 20 MHz. The pulse repetition rate of the ultrasonic pulse was 1 kHz, which was synchronized to the data-acquisition rate. The test sample was set to the sample holder vertically and connected to the water tank to fill its cooling tube with water. The ultrasonic probe was inserted into the cooling tube of the mock-ups from the top of the sample holder.

When the joint interface has good metallurgical connection, the ultrasonic pulse emitted from the transducer can be transferred from the cooling tube into the CFC monoblock with negligible reflection at the joint interface. If pores, voids, or defects exist at the joint interface, the reflection becomes stronger or dominant. The intensity of the reflection at the joint interface was mapped according to the coordinates of ultrasonic scanning to recognize the joint defect.

2.5. Results of NDE with ultrasonic wave

Fig. 5 shows the result of the ultrasonic testing on the joint interface of the mock-up of TP-1. The scanning steps were 0.5 mm in the axial direction (z) and 0.5° in the rotational direction (θ). The position of the ion beam during HHF testing (cf. following section) corresponded to an angle of 180°.

The gaps between the tiles are clearly distinguished. In this figure, the white region represents a strong signal of the ultrasonic pulse reflected from the joint defect; the black region represents a weak signal, which means the joint interface is sound. The results of the ultrasonic testing show that tiles #3 and #4 have joint defects positioned at about 180° as indicated with arrows in Fig. 5. The maximum size of the joint defects in tiles #3 and #4 are estimated to be 15% and 20% of perimeter of the joint interface, i.e. the angles of the defects are estimated to be 54° and 72°. These characteristics of the joint interface correspond to those recognized with the thermography. Although in tiles #1, #2 and #5, the joint defects at the heated side were not observed like #3 and #4, weaker reflected signals were observed in the rear side of the cooling tube at about 0°, typically, as encircled in the figure. Since thermography was performed

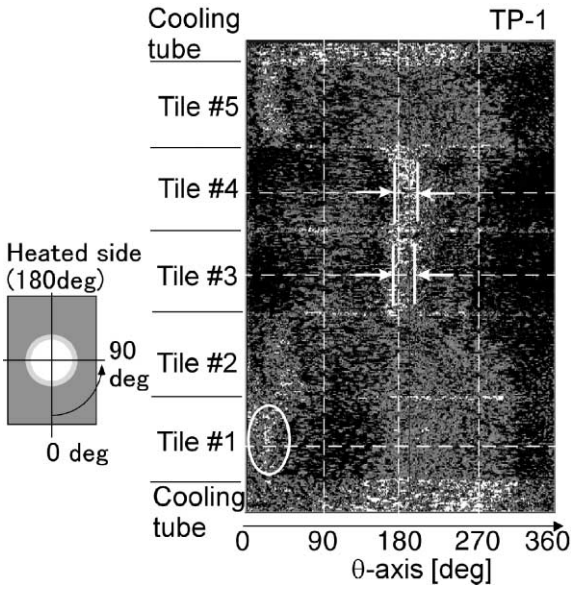

Fig. 5. Mapping of the intensity of the ultrasonic signal after reflection at the joint interface of the CFC monoblocks and the copper cooling tube of TP-1. White region represents high-reflected signal region.

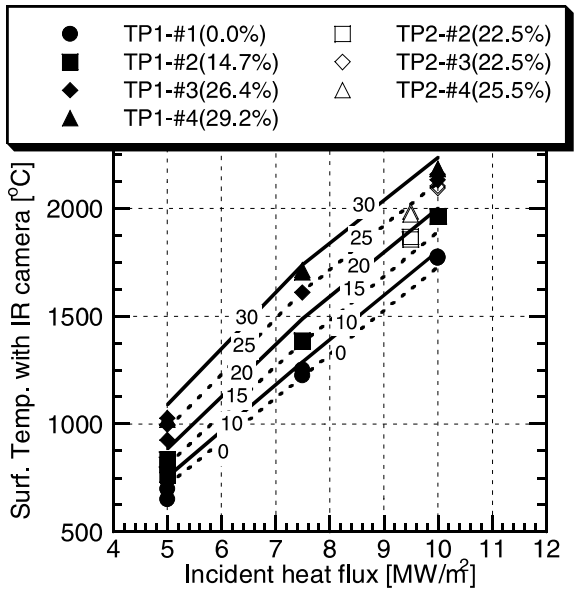

Fig. 6. Results of screening test on the mock-ups TP-1 and TP-2. Percentages in the parentheses indicate the joint defect estimated with the thermography. Solid and dotted lines represents the results of FE calculation with assumption of joint defects. Numerical values on the lines are the joint defect size used in the analyses.

from the upper surface only, these joint deflects at 0° could not be detected by the IR-techniques.

3. Examination of NDE characterization of the joint interface with HHF test and cross-sectional observation

To examine the results of NDE on the joint interface of the mock-up, HHF tests on the mock-ups and cross-sectional observations of the joint interface were carried out. HHF tests on the mock-ups with CFC monoblock were carried out in an ion beam facility (PBEF) of JAERI [11]. The experimental conditions were as follows: (1) the axial flow velocity was 10 m/s, (2) the local pressure at the center of the mock-up was about 1 MPa, (3) inlet water temperature was room temperature, (4) the peaked heat fluxes were at maximum 5, 7.5 and 10 MW/m^2.

3.1. Results of HHF tests of the mock-ups and comparison of NDE results with HHF tests

Fig. 6 shows the maximum temperatures of each tile of the mock-ups as a function of the incident heat flux. These results are compared with the thermal analyses assuming the joint defect in the heated side of the joint interface. For instance, tile #1 of the mock-up TP-1 is estimated to have no joint defect. Its thermal response is of good agreement with that predicted by the numerical analyses [8]. For the other tiles, tile #3 and #4, which were estimated to have a joint defect size from 26% to 29%, their surface temperatures ranged in the value predicted with assumption of the 25–30% joint defect size. The good relationship between the results of the HHF tests and those of the NDE with thermography can be confirmed. From the results of the HHF tests, it can be concluded that the joint defect size affecting the surface temperature can be estimated with the thermography.

3.2. Cross-sectional examination of the joint interface

Fig. 7 shows the macroscopic observations of the joint interfaces of tiles #1, #3 and #4 of the mock-up TP-1. The observations of the cross-sections are indicated in the figure with dotted lines in Fig. 5. The results of the ultrasonic testing indicated that tiles #3 and #4 have joint defects at an angle around 180° and good joint conditions in the opposite side. From the cross-sectional observations of tiles #3 and #4, the joint defects were observed at the heated side (around 180°). On the contrary, in tile #1, some pores or small void-like brazing defects were observed at the rear side (around 0°), which correspond to the results obtained with the ultrasonic testing as indicated with a circle in Fig. 5. From the results of the thermography, the joint defects at the rear side could not be clearly detected, especially such pores in the joint defects. It is supposed that these

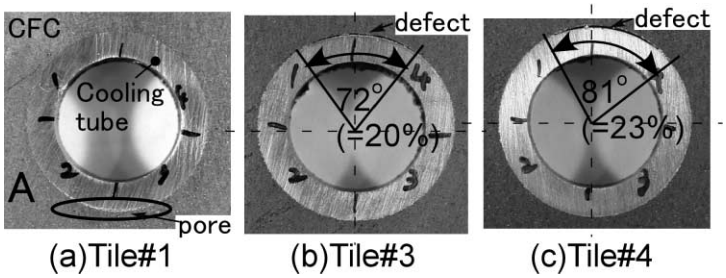

Fig. 7. Cross-sectional observation and size estimation of the joint defect of tiles #1, #3 and #4 of the mock-up TP-1.

void-like defects have a less effect on the overall heat transfer characteristics of the tile than the joint defects in tiles #3 and #4 did.

To evaluate the detection accuracy of two NDE methods, the size of joint defects was measured through the cross-sectional observations. The joint defect size of tiles #3 and #4 of the mock-up TP-1 are estimated to be 20% and 23% of the perimeter of the joint interface, which corresponds to angles of 71° and 82°. By comparison with these results, the NDE with ultrasonic wave predicted that the joint defects size of tile #3 and #4 were 15% and 20%, i.e., 75% and 87% of the actual observed sizes. On the contrary, the NDE using thermography predicts that the size was about 26% and 29%, about 1.3 times larger than the results of the cross-sectional observations. From these results, the ultrasonic testing estimates that the joint defect size is smaller than the actual size. The thermography estimates a larger joint defect. In the ultrasonic technique, the local joint defect size can be recognized; on the contrary, the thermography predicts the overall characteristics of the joint interface.

4. Summary of NDE and HHF tests on CFC monoblock mock-up

Two NDE methods have been examined using the mock-ups with CFC monoblock armor brazed on a Cu cooling tube. One is based on the ultrasonic method and the other is based on the thermographic method. The former method can reveal the local characteristics of the joint defects while the latter estimates the overall characteristics.

High heat flux tests up to 10 MW/m^2 were performed to examine the thermal response of the mock-ups with initial joint defects which were characterized with both NDE methods. The experimental values of the surface temperature are in good agreement with those based on the results of NDE.

From the comparison of cross-sectional observations with the results of NDE, the ultrasonic testing estimated the joint defect size to be 75–86% of the actual sizes and the thermography estimated the joint defect to be 1.3 times larger than the actual sizes. From the results of the cross-sectional observations and the HHF tests, it can be concluded that both NDE techniques have sufficient accuracy to predict the surface temperature of the HHF components.

Acknowledgements

The authors wish to thank the member of the Neutral Beam Injection Heating Laboratory for their valuable discussions and support for carrying out experiments. The authors also acknowledge Dr S. Matsuda and Dr M. Seki for their support and encouragement.

References

[1] R. Tivey, M. Akiba, D. Driemeyer, I. Mazul, M. Merola, M. Ulrickson, Fus. Eng. Des. 55 (2001) 219.
[2] I. Šmid, E. Kny, M. Scheerer, P.A. Hahn, G. Korb, J. Linke, G. Vieider, Fus. Eng. Des. 42 (1998) 511.
[3] E. Di Pietro, E. Visca, A. Orsini, M. Sacchetti, T.M.R. Borruto, P. Varone, R. Vesprini, in: Proceedings of 16th IEEE/NPSS Symposium on Fusion Engineering (SOFE95), 1995, p. 190.
[4] R. Mitteau, S. Berrebi, P. Chappuis, Ph. Darses, A. Dufayet, L. Garampon, D. Guilhem, M. Lipa, V. Martin, H. Roche, in: C. Varandas, F. Serra (Eds.), Fusion Technology 1996, 1997, p. 443.
[5] J. Schlosser, P. Chappuis, A. Durocher, L. Moncel, P. Garin, Phys. Scripta T 91 (2001) 94.
[6] M. Scheerer, H. Bolt, A. Gervash, J. Linke, I. Šmid, Phys. Scripta T 91 (2001) 98.
[7] F. Escourbiac, P. Chappuis, J. Schlosser, et al., Fus. Eng. Des. 56&57 (2001) 285.
[8] K. Ezato, M. Dairaku, M. Taniguchi, K. Sato, M. Sato, M. Akiba, JAERI-Tech., Japan Atomic Energy Research Institute, submitted for publication.
[9] K. Ezato, M. Taniguchi, K. Sato, M. Sato, M. Akiba, Phys. Scripta T 91 (2001) 110.
[10] Hibbit, Karlson and Sorenson, 'ABAQUS user's manual 5.8', Providence, RI, USA, 1996.
[11] J. Boscary, M. Araki, S. Suzuki, K. Ezato, M. Akiba, Fus. Technol. 35 (1999) 289.